Thieno[3,2-*b*]thiophene-diketopyrrolopyrrole Containing Polymers for Inverted Solar Cells Devices with High Short Circuit Currents

Hugo Bronstein, Elisa Collado-Fregoso, Afshin Hadipour, Ying W. Soon, Zhenggang Huang, Stoichko D. Dimitrov, Raja Shahid Ashraf, Barry P. Rand, Scott E. Watkins, Pabitra S. Tuladhar, Iain Meager, James R. Durrant, and Iain McCulloch*

The synthesis and characterization four diketopyrrolopyrrole containing conjugated polymers for use in organic photovoltaics is presented. Excellent energy level control is demonstrated through heteroatomic substitution whilst maintaining similar solid state properties as shown by X-ray diffraction and atomic force microscopy. Inverted solar cells were fabricated with the best devices having short circuit currents exceeding 16 mA cm^{-2} and efficiencies of over 5% irrespective of whether [6,6]-phenyl-C_{61}-butyric acid methyl ester ($PC_{60}BM$) or [6,6]-phenyl-C_{71}-butyric acid methyl ester ($PC_{70}BM$) is used. Transient absorption spectroscopy on the bulk heterojunction blends shows efficient charge photo-generation, with the variations in short circuit current correlated to the energetic offset between polymer and fullerene.

1. Introduction

Low band-gap donor–acceptor conjugated co-polymers have shown great promise in the field of organic photovoltaics. Their ability to harvest a large proportion of the solar flux has resulted in power conversion efficiencies (PCE) exceeding 7%.[1–16] Diketopyrrolopyrrole (DPP) containing polymers are an important constituent of this class, with efficiencies in excess of 5% being reported by several research groups.[17–21] The extremely electron-deficient nature of the DPP unit allows access to ultra-low band-gap materials when co-polymerized with electron rich units, such as thiophenes through donor-acceptor type orbital hybridization.[17] Furthermore, the DPP unit can host two pendant alkyl chains giving the resulting polymers solubility and processability which are necessary in order to achieve low cost, large area solar cells via solution-based printing techniques. Finally, DPP containing conjugated materials typically have extremely high hole mobilities which could assist with charge extraction, minimizing recombination losses in photovoltaic devices.[18,22]

Inverted solar cell architectures are becoming increasingly attractive by allowing more air stable, higher work function metal electrodes (e.g., Ag) to be used, resulting in a longer-lived device.[23] A further benefit of this structure is that it facilitates the fabrication of tandem solar cells.[24–28] For these to operate efficiently, it is necessary to have two materials with complementary absorption in the visible spectrum. Typically, a wide band gap material such as poly(3-hexylthiophene) (P3HT) is used to absorb the solar spectrum in the 300–600 nm range, and a red-absorbing material is required to absorb the low energy photons. The low band-gap materials must also demonstrate high fill factors and preferably be able to achieve high efficiencies without the use of [6,6]-phenyl-C_{71}-butyric acid methyl ester ($PC_{70}BM$), as this acceptor is not a complementary absorber to P3HT. Due to their low band gap absorption, DPP containing polymers are excellent candidates to construct high efficiency tandem solar cells.[12,29,30]

We previously reported the synthesis and characterization of poly-thieno[3,2*b*]thiophene-diketopyrrolopyrrole-co-thiophene (DPPTT-T), and demonstrated its high performance in a standard solar cell architecture.[18] Its strong absorption in the red part of the solar spectrum makes it a suitable candidate for use in inverted solar cells, with an eventual aim to use this class of materials in tandem solar cells. Heteroaromatic substitutions are a common method to manipulate the electronic and physical properties of a conjugated polymer, and this design strategy can be used to fine tune the frontier orbital energy levels to create materials with complementary absorption.[31–33] With this in mind, two novel selenium containing polymers

Dr. H. Bronstein,
Department of Chemistry
University College London
London WC1H 0AJ, UK
E-mail: h.bronstein@ucl.ac.uk
E. Collado-Fregoso, Y. W. Soon, Z. Huang,
Dr. S. D. Dimitrov, Dr. R. S. Ashraf, Dr. P. S. Tuladhar,
I. Meager, Prof. J. R. Durrant, Prof. I. McCulloch
Department of Chemistry and Centre for Plastic Electronics
Imperial College London
London SW7 2AZ, UK
Dr. A. Hadipour, Dr. B. P. Rand
IMEC, Kapeldreef 75, B-3001, Leuven, Belgium
Dr. S. E. Watkins
CSIRO Materials Science and Engineering
Melbourne, VIC 3169, Australia

DOI: 10.1002/adfm.201300287

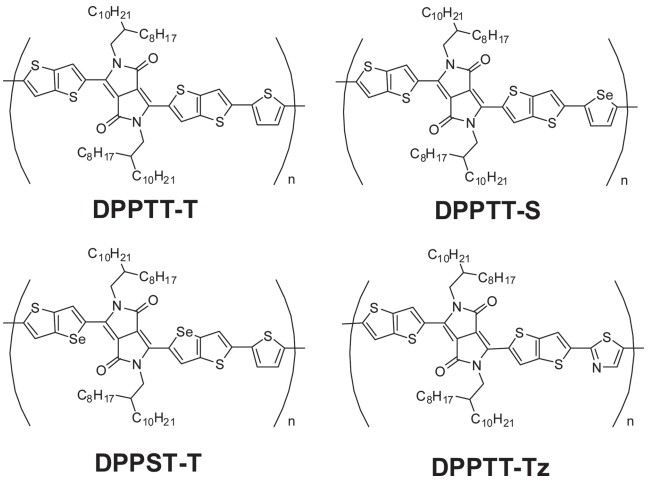

Figure 1. Structures of DPP containing polymers.

analogues were synthesized; the first by replacing the thiophene co-monomer with selenophene (DPPTT-S); the second by replacing the two sulphur atoms nearest the DPP core with selenium (DPPST-T). Finally, the thiophene co-monomer was replaced with the more electron poor thiazole unit (DPPTT-Tz). Structures are shown in **Figure 1**.

2. Results and Discussion

All polymers were synthesized by microwave-assisted stille couplings and isolated as green fibers with high molecular weights (**Table 1**) and with excellent mass recovery. Detailed synthetic procedures can be found in the Supporting Information. The polydispersities (PDI) of DPPTT-T, DPPST-T, and DPPTT-Tz are relatively high as it was not possible to remove all of the lower molecular weight oligomeric material through Soxhlet extraction (although it was possible to attain higher molecular DPPTT-T than previously reported through the use of multiple extraction solvents), which can be observed in the gel-permeation chromatography (GPC) elugram (**Figure 2**c). DPPTT-S and DPPTT-Tz were fully soluble in chlorinated solvents such as chloroform and chlorobenzene, whereas DPPTT-T and DPPST-T were only soluble in chlorobenzene and dichlorobenzene. We attribute the difference in solubility to the increased presence of oligomeric impurities disrupting aggregation in DPPTT-S and DPPTT-Tz.

The solution and thin film UV-Vis spectra of the four polymers is shown in Figure 2. All materials have low band-gaps with absorption maxima at a wavelength of $\lambda \approx 800$ nm. Thin-films of all the polymers demonstrated a red-shift in absorption onset, compared to their respective solution spectra, attributed to solid state packing effects, and more bi-modal absorption maxima, attributed to the appearance of vibrational fine structure. The frontier molecular orbital energies measured by photoelectron spectroscopy in air (UV-PES) and the absorption onsets from the UV-Vis spectra are compared to the predicted energies calculated using (time dependent) density functional theory DFT/TDDFT with a 6–31g* basis set are

Table 1. Physical properties of the polymers studied in this work.

Polymer	M_n [kDa][a)]	M_w [kDa][a)]	PDI[a)]	HOMO [eV][b)]	LUMO [eV][c)]	Band gap [eV][c)]
DPPTT-T	35	150	4.3	–5.1	–3.7	1.40
DPPTT-S	32	176	5.5	–5.1	–3.73	1.37
DPPST-T	90	185	2.0	–5.0	–3.75	1.35
DPPTT-Tz	25	250	10	–5.2	–3.77	1.43

[a)]Determined by GPC(CB) against PS standards; [b)]determined by photoelectron spectroscopy in air (UV-PES); [c)]determined from absorption onset in thin film UV-Vis spectra.

shown in Figure 2d. Firstly, it can be seen that the calculated energy levels reproduce the observed experimental trends, validating the use of this method to aid analysis of heteroatom effects on the HOMO and LUMO. Replacing the thiophene co-monomer DPPTT-T with selenophene DPPTT-S only marginally alters the highest occupied molecular orbtial (HOMO) of the polymer. However, the lowest unoccupied molecular orbital (LUMO) is significantly lowered leading to an overall red-shift in the polymer absorption. This effect is commonly observed upon replacing sulphur with selenium, and is typically attributed to the lack of electron density contribution of the selenium to the HOMO, whilst its lower ionization potential leads to a lowering of the LUMO energy.[33] However, comparing DPPTT-T and DPPST-T, the opposite effect is observed. In this case, replacing the two closest sulphur atoms to the DPP core with selenium results in a raising of the HOMO energy level, with little impact on the LUMO. The HOMO and LUMO distributions of all polymers (Supporting Information, S4) show no significant differences, indicating that it is not a direct electronic contribution from the selenophene atom causing these differences. However, it has also been shown that the larger size of the selenium atom in selenophene can reduce C–C bond distances to neighboring substituents.[34] The C–C bond linking the thieno-selenophene unit to the DPP core in DPPST-T is reduced in comparison to DPPTT-T and DPPTT-S (Supporting Information, S5). As the HOMO is predominantly anti-bonding along the polymer backbone axis, this reduced distance could lead to energetic destabilization, due to its greater repulsion. However, a similar bond length reduction is also observed comparing the DPPTT-T and DPPTT-S structures, and no destabilization of the HOMO energy level is observed. It is likely that a complex interplay of factors including ionization potential, electron affinity, and size is responsible for the variations in the orbital energy levels. DPPTT-Tz, on the other hand, has both lower HOMO and LUMO energy levels, due to electron deficiency of the thiazole unit. Furthermore, there is a widening of the band-gap in this material as the HOMO is affected to a greater extent. Similar effects have been observed by introducing an aromatic nitrogen atom into other conjugated materials.[32]

Inverted solar cells were fabricated with all four materials using a device architecture of indium tin oxide (ITO)/TiO_x (10 nm)/Active layer (95–100 nm)/MoO_3 (10 nm)/Ag (for fabrication details, see Supporting Information).[35] The current density versus voltage (*J*–*V*) curves and external quantum efficiency

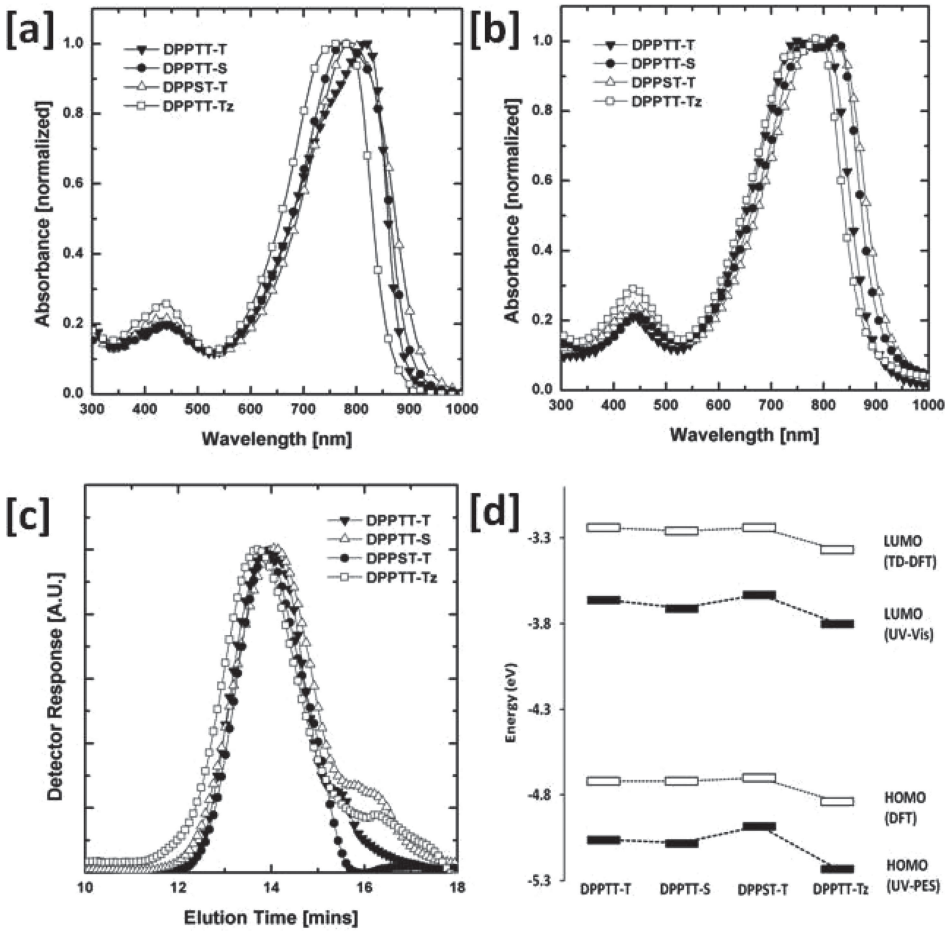

Figure 2. a) Solution UV-Vis spectra recorded in chlorobenzene. b) Thin film (spun from chlorobenzene 5 mg mL^{-1}, 1000 RPM) UV-Vis spectra. c) GPC elution curves in chlorobenzene 80 °C. d) Measured (UV-PES and UV-Vis) and calculated (DFT and TD-DFT using B3LYP/6.31g* basis set) HOMO and LUMO energy levels.

(EQE) spectra are shown in **Figure 3** and the photovoltaic parameters are presented in **Table 2**. Due to spectral mismatch owing to the broad and near-infrared absorption (particularly at $\lambda > 800$ nm) of the solar cells, the corrected short-circuit current density (J_{SC}) derived from the integrated EQE spectra and the subsequently corrected PCE are also given. Devices utilizing DPPTT-T produce the highest efficiencies among the polymers studied here, with an open circuit voltage (V_{OC}) of 0.56 V, fill factor (FF) of approximately 60%, and J_{SC} greater than 16 mA cm^{-2} using either [6,6]-phenyl-C61-butyric acid methyl ester ($PC_{60}BM$) or $PC_{70}BM$. Replacement of the thiophene co-monomer in DPPTT-T with selenophene DPPTT-S resulted in a solar cell devices with a similar V_{OC} (0.55 V), but a lower J_{SC}. The use of DPPST-T results in a significantly reduced V_{OC} (0.49 V) due to its raised HOMO as was observed by PESA. Finally, devices made using DPPTT-Tz had a much larger V_{OC} as expected from its lower HOMO energy level, but suffer from poor FF and lower J_{SC}. It is interesting to note that all materials result in similar performance despite the choice of $PC_{60}BM$ versus $PC_{70}BM$. The EQEs (Figure 3c,d) show that when $PC_{60}BM$ is used, the maximum percentage of charge photogeneration for light absorbed by the polymer is higher than when $PC_{70}BM$ is used. However, when $PC_{70}BM$ is used as the acceptor, despite the lower maxima, the absorbance and contribution of the fullerene to charge generation compensates for this loss in polymer signal. The fact that both acceptors can be used interchangeably to obtain similar performance is beneficial, as it allows the materials to be used with greater flexibility. It is also interesting to note that in the case of DPPST-T, the EQE demonstrates its decreased bandgap by having a red-shifted absorption onset that correlates well with the UV-Vis spectrum. However, the onset of DPPTT-S is identical to that of DPPTT-T despite it having a significantly reduced bandgap according to its UV-Vis spectra. In particular, DPPTT-T and DPPST-T show promising characteristics for incorporation as a low bandgap component within tandem solar cells. Conventional arcitecture solar cells were also manufactured with their performance being extremely similar to the inverted cells (see Supporting information, S6).

It was hypothesized that the lower FF of the DPPTT-Tz devices was due to the presence of oligomeric impurities resulting in sub-optimal active layer morphologies. The material displayed an extremely broad PDI of 10, and a significant hump can be observed in the low molecular weight region of

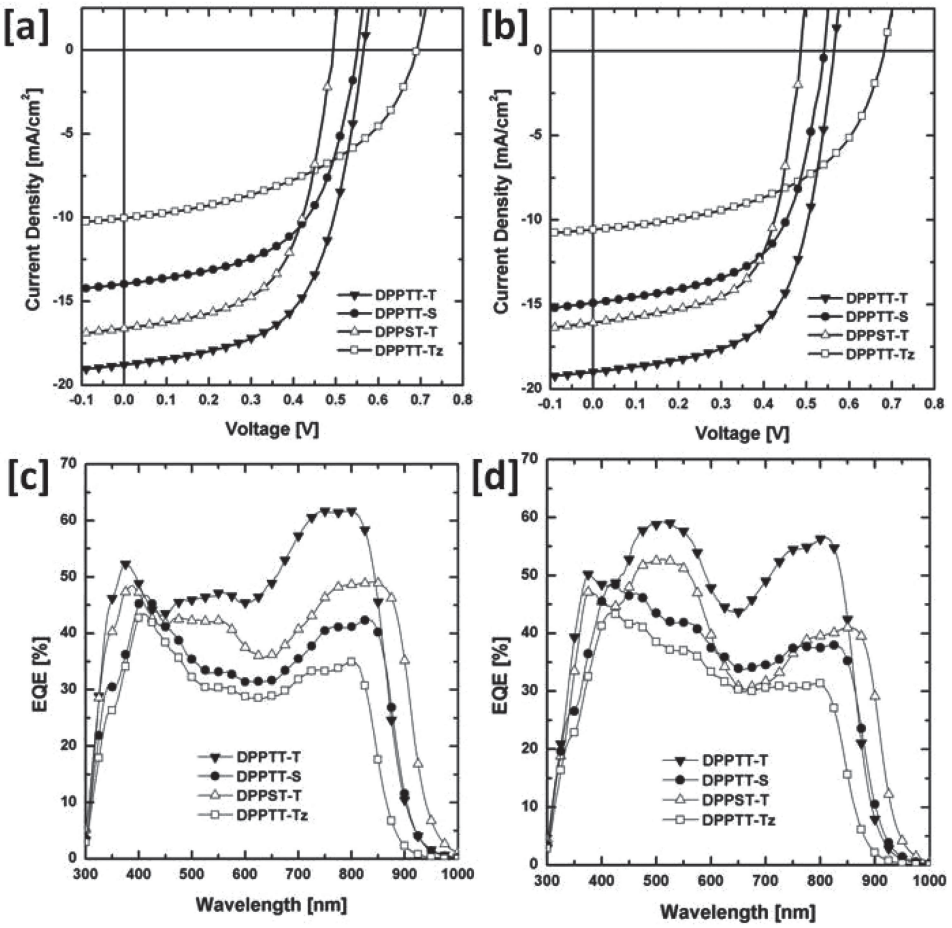

Figure 3. Current density vs. voltage characteristics of a) polymer:$PC_{60}BM$ devices, and b) polymer:$PC_{70}BM$ devices. External quantum efficiency (EQE) spectra of c) polymer:$PC_{60}BM$ devices, and d) polymer:$PC_{70}BM$ devices.

the elugram (Figure 2c). It is possible that these oligomeric residues act as traps in the device leading to reduced charge extraction and/or increased recombination. Furthermore, large PDIs are often observed in DPP based polymer and are sometimes attributed to solution phase aggregation and sometimes oligomeric impurities.[36–39] Therefore it was of interest to us investigate the origin and effect of the broad PDI on device efficiency. A sample of the DPPTT-Tz polymer was further purified by recGPC using chlorobenzene as a solvent and an Agilent PLgel 10 μm MIXED-D column allowing the isolation of a high molecular weight, narrow polydispersity fraction. **Figure 4**a shows the GPC elugram before and after fractionation, clearly demonstrating the removal of the lower molecular weight oligomeric impurities, and a highly symmetrical elution profile indicating that the origin of the large PDI was not due to solution aggregation. The molecular weight of the isolated fractionated material was M_n = 42 kDa and M_w = 74 kDa. Higher molecular

Table 2. Solar cell parameters (open-circuit voltage (V_{OC}), short-circuit current density (J_{SC}), fill factor (FF), and power conversion efficiency (PCE)) of the various solar cells, as well as the J_{SC} and PCE expected from integration of the external quantum efficiency (EQE) spectra of Figure 3 with the AM1.5G irradiance spectrum.

Polymer	Acceptor	V_{OC} [V]	J_{SC} [mA cm^{-2}]	FF	J_{SC} (EQE) [mA cm^{-2}]	PCE [%]
DPPTT-T	$PC_{60}BM$	0.56	18.9	59	16.6	5.5
	$PC_{70}BM$	0.56	19.0	61	16.5	5.6
DPPTT-S	$PC_{60}BM$	0.55	14.3	57	12.1	3.8
	$PC_{70}BM$	0.54	14.9	60	12.7	4.1
DPPST-T	$PC_{60}BM$	0.49	16.3	61	14.8	4.4
	$PC_{70}BM$	0.49	16.4	60	14.0	4.1
DPPTT-Tz	$PC_{60}BM$	0.68	10.0	47	10.0	3.2
	$PC_{70}BM$	0.68	10.6	52	10.4	3.7

Table 3. Solar cell parameters (open-circuit voltage (V_{OC}), short-circuit current density (J_{SC}), fill factor (FF), and power conversion efficiency (PCE)) of the fractionated DPPTT-Tz based solar cells, as well as the J_{SC} and PCE expected from integration of the external quantum efficiency (EQE) spectra of Figure 4 with the AM1.5G irradiance spectrum

Polymer	Acceptor	V_{OC} [V]	J_{SC} [mA cm^{-2}]	FF	PCE [%] (from EQE)
Unfractionated	$PC_{70}BM$	0.68	9.35	48	3.1
Fractionated	$PC_{70}BM$	0.70	10.4	63	4.6

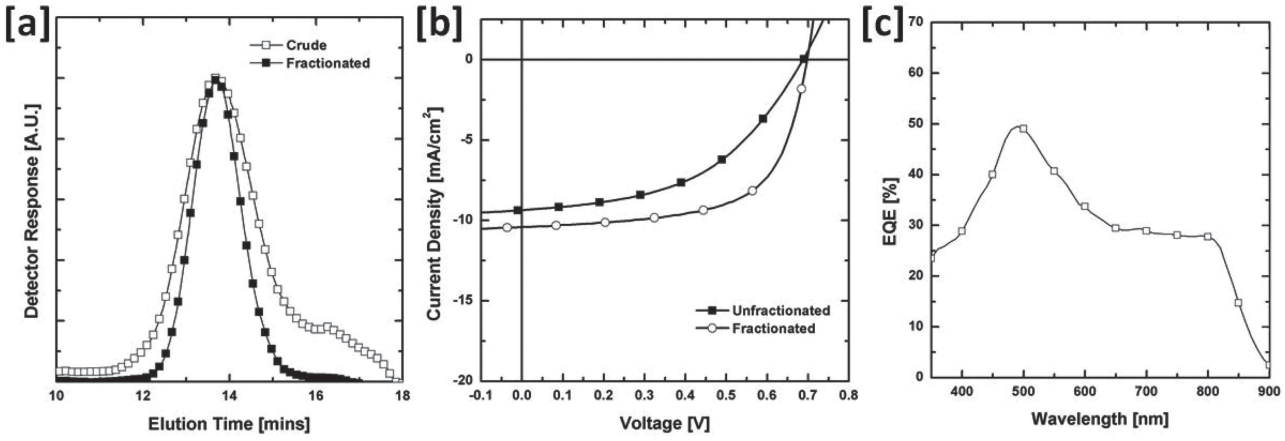

Figure 4. a) GPC elution curves of pre and post fractionated DPPTT-Tz in chlorobenzene 80 °C. b) Current density vs. voltage characteristics of pre- and post-fractionated DPPTT-Tz:$PC_{70}BM$ device. c) External quantum efficiency (EQE) spectra of DPPTT-Tz:$PC_{70}BM$ device.

weight fractions were also isolated but their low solution processability prevented their functional use. In order to test whether the origin of the low FF is due to oligomeric residue, conventional solar cells were fabricated using the same active layer processing conditions as mentioned previously. Due to the small quantity of material that can be purified by recGPC it was not possible to construct inverted solar cells. The solar cells characteristics of the pre-and post-fractionated devices are shown in Figure 4b,c and the device data is tabulated in **Table 3**. The material retains its high open circuit voltage (≈0.7 V) as a result of the electron deficient nature of the thiazole repeat unit. Interestingly, the short circuit current density is not increased at all relative to the original devices. However, the fill factor has been increased to an impressive 63%, demonstrating that the removal of the olgomeric impurities results in a better functioning device. It is also interesting to note that the overall shape of the EQE has not been affected, in particular, the relatively low contribution (≈30% EQE) to the photocurrent from the polymer absorption (600–900 nm). Henceforth, the fractionated DPPTT-Tz sample was used for all further studies outlined below.

In order to investigate the origin of the varying solar cell short circuit currents from the four polymers, a structural study was undertaken to ascertain whether the differences could be due to differing microstructure.

Figure 5a shows the XRD spectra of drop cast thin films of the four polymers. The (100) and (200) diffraction peaks can clearly be seen, indicating that in neat film all four polymers adopt a lamellar type packing motif similar to P3HT. The d-spacing for all four polymers is approximately 2.2 nm. Figure 5b shows the XRD of a drop cast 1:2 polymer:$PC_{70}BM$ blend thin film. Interestingly, the presence of the fullerene does not fully disrupt the crystallinity of the polymer as is often observed in annealed blends of P3HT:PCBM.[40] The presence of PCBM can clearly be seen by the peak at ≈19°. The similarity of all four polymers in both neat film and blend is perhaps not too surprising considering their structural resemblance. Therefore, the XRD spectra imply that differences in the solid state microstructure are unlikely to account for the observed differences in the measured photocurrent.

To further confirm the absence of a structural origin for the varying photocurrents, atomic force microscopy (AFM)

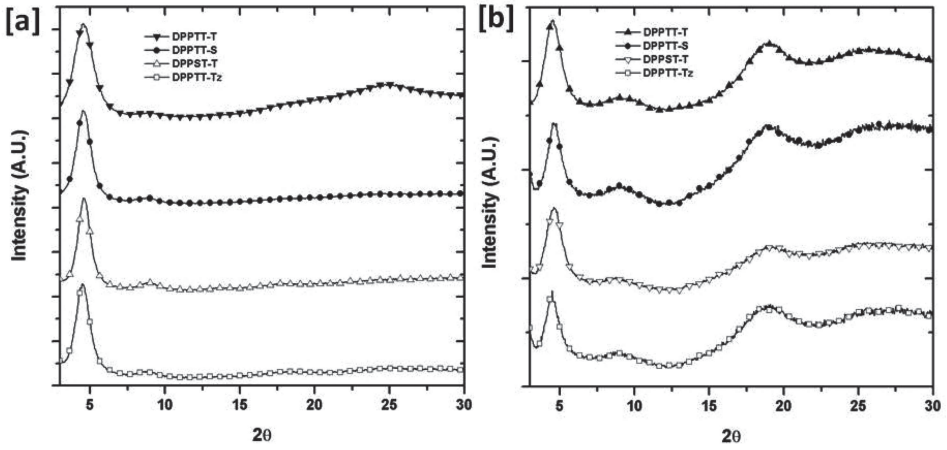

Figure 5. Thin film (drop cast film) XRD profile of a) neat polymers and b) polymer:$PC_{70}BM$ blends.

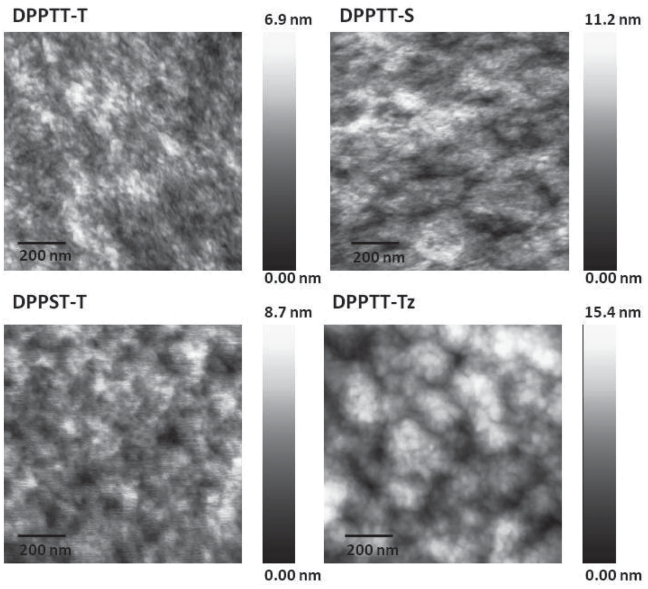

Figure 6. AFM (tapping mode) of polymer:$PC_{70}BM$ blend thin films (spin coated).

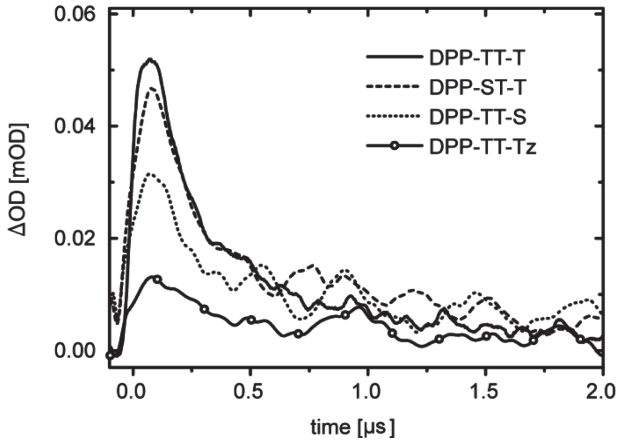

Figure 7. Transient absorption decays of thin films of polymer:$PC_{70}BM$ blends with 1:1 weight ratio. The films were excited at the maximum of polymer absorption and the polymer polaron band was probed at 1200 nm.

(tapping mode) images of 1:2 polymer:$PC_{70}BM$ blend thin films were obtained (**Figure 6**). The films were produced in an identical manner to the active layer in the solar cell. In the phase images (Supporting Information, S7), a homogeneous feature is observed across all the samples with DPPTT-Tz being slightly less comparable to the others. The nanoscale phase separation of all 4 materials appears to be fairly similar, with observable features having approximately <25 nm size. In addition, the contrast between the domains observed which contain mostly polymers or fullerene is weak. This suggests that purities of the domains are similar and the degree of polymers/fullerenes mixing is on a scale which cannot be precisely measured by AFM. Furthermore, all blends demonstrate similar surface roughness.

We were interested in studying whether the observed reduction in short circuit current for polymers DPPTT-S, DPPST-T, and DPPTT-Tz relative to DPPTT-T could be due to their lower lying LUMO levels reducing the efficiency of photoinduced charge separation. To address this, we employed nano- to millisecond transient absorption spectroscopy (TAS) of thin films of polymer:$PC_{70}BM$ blends. Details about the experimental set-up and data collection conditions can be found in the Supporting Information, S8. All transients exhibited power-law decays assigned, as previously,[41,42] to non-geminate recombination of dissociated polarons in the presence of an exponential tail of the density of states. Data were collected under low excitation density conditions (≈1.6 μJ cm^{-2}) to avoid significant non-geminate recombination prior to our instrument response (≈200 ns full-width half maximum, FWHM). The amplitude of these transient decays is an indicator of the quantum yield of dissociated charges generation by optical excitation. We have previously shown this assay of the yield of dissociated charges can exhibit a good correlation with photocurrent generation efficiency in devices.[43] For all polymers, reasonably strong transient absorption signals were observed, indicating that despite the low lying polymer LUMO levels, charge photogeneration is efficient. A closer consideration of the transient kinetics plotted in **Figure 7** indicates that their amplitude shows a good correlation with the short circuit photocurrent data shown in Table 2. It can thus be concluded that the lower photocurrents observed for DPPTT-S, DPPST-T, and DPPTT-Tz relative to DPPTT-T indeed result primarily from lower yields of photoinduced charge separation.

In order to evaluate whether the variation in charge separation yields and photocurrent densities observed for these polymers can be assigned to the differences in LUMO–LUMO energy offset, we consider the correlation between the energy driving charge separation and the yield of polarons as measured by our transient absorption (TA) studies. Consistent with our previous studies,[41] we define the relative energy for charge separation as $\Delta E_{CS}^{rel} = E_S - (IP_D - EA_A)$ where E_S, IP_D and E_A are the donor exciton energy, ionization potential of the donor, and electron affinity of the acceptor respectively. We note that the values for ΔE_{CS}^{rel} should be considered as relative rather than absolute, as there is significant uncertainty in the values of the energies used (e.g., the data shown use an electron affinity of 4.1 eV for $PC_{70}BM$; however we note that data from the literature ranges from 3.6 to 4.1 eV).[44–47]

Figure 8 shows a plot of optical density change (ΔOD) of polymer/$PC_{70}BM$ blend films measured at 100 ns, as a function of ΔE_{CS}^{rel}. We have included therein data points for three additional DPP-based polymers in order to extend the range of (ΔE_{CS}^{rel}) values studied. Details of these three additional polymers are given in the Supporting Information, S9. It is evident that we observe a correlation between the yield of positive polarons and (ΔE_{CS}^{rel}) for the seven DPP-based polymer/fullerene blend films. This correlation is analogous to what we have observed previously for other thiophene-based polymeric systems,[48] in which larger driving energies for charge separation were associated with higher charge separation efficiencies.

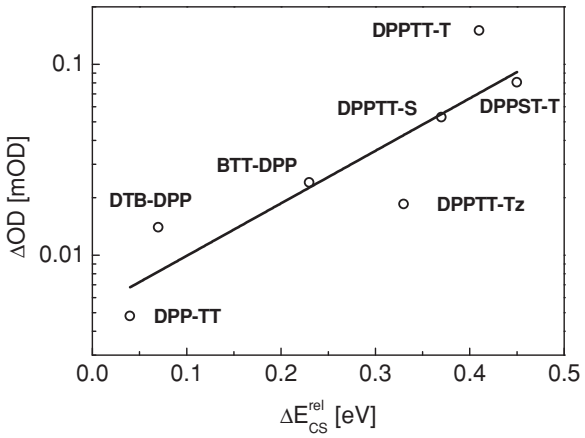

Figure 8. Transient optical density of polymer/fullerene blend films. Signals were taken at 100 ns, normalized for absorption and for excitation density at 1 μJ cm^{-2}. ΔE_{CS}^{rel} was calculated as $E_S - (IP_D - EA_A)$, see text. The electron affinity for $PC_{70}BM$ was taken to be 4.1 eV. For DPP-TT, BTT-DPP and DTB-DPP see Supporting Information, S9.

It is also consistent with an analogous analysis of device EQE versus energy offset by Li et al. for several alternative DPP-based BHJ devices.[20] We have previously proposed that this dependence upon energy offset derives from the need for excess energy to avoid the formation of bound interfacial charge transfer states.[49] We thus conclude that the lower photocurrent densities observed for DPPTT-S and DPPTT-Tz polymers studied herein indeed result from LUMO levels which are too low to drive charge separation from polymer excitons. In contrast, both DPPST-T and DPPTT-T have higher predicted driving energies, and correspondingly higher ΔOD signal amplitudes and photocurrent densities.

We note that the analysis we have undertaken here is only concerned with charge generation from polymer excitons. As we have reported previously, such DPP based polymers exhibit rather large driving forces for hole transfer from fullerene excitons (i.e., large HOMO–HOMO offsets) and consequently can exhibit efficient charge generation following fullerene light absorption.[50]

It is also apparent from Figure 8 that the LUMO energy offset required to generate charges in DPP-based polymers implies a significantly smaller driving force than that needed to obtain the same yield of positive polarons for thiophene based polymers such as P3HT.[41] A possible explanation to this observation might be related to the increased charge transfer (CT) character of the electronic transitions in donor–acceptor polymers herein presented, as we have previously proposed for other donor–acceptor polymers. This charge transfer character may facilitate the dissociation of charge carriers, either by increasing the local polarizability or by reducing the Coulomb binding energy of interfacial charge transfer states.[51] We also note that DPP-based polymers exhibit particularly high carrier mobilities, which may also contribute to the ability of these polymers to generate high charge photogeneration yields and short-circuit currents even with relatively low LUMO offsets.[20]

3. Conclusions

We have demonstrated an excellent control of energy level alignment in a series of four DPP containing polymers. Replacement of thiophene with selenophene was found to either raise the HOMO or lower the LUMO depending on its location resulting in a material with a narrower band-gap. Replacement of the thiophene co-monomer with thiazole resulted in a substantial decrease in the HOMO energy level of the polymer, with a net blue-shift in absorption. Inverted solar cells were fabricated with all materials with the best device having a short circuit current exceeding 16 mA cm^{-2} and an overall PCE of 5.6%. Transient absorption spectroscopy on polymer/fullerene blend films demonstrated efficient charge-photogeneration. Moreover, it has been shown that the reduction in photocurrent observed for DPPTT-S, DPPST-T, and DPPTT-Tz relative to DPPTT-T can be mainly ascribed to a reduction in charge separation efficiency related to an insufficient LUMO–LUMO offset. Two of the materials demonstrated almost ideal characteristics for use in tandem solar cells, due to their near infrared absorption, high fill factors, and high photocurrent.

Supporting Information

Supporting Information is available from the Wiley Online Library or from the author.

Acknowledgements

The authors thank the X10D, ONE-P, EPSRC, APEX, Scallop, and CONACyT for financial support.

Received: January 24, 2013
Revised: March 20, 2013
Published online: June 17, 2013

[1] C. M. Amb, S. Chen, K. R. Graham, J. Subbiah, C. E. Small, F. So, J. R. Reynolds, *J. Am. Chem. Soc.* **2011**, *133*, 10062.
[2] Y. Liang, L. Yu, *Acc. Chem. Res.* **2010**, *43*, 1227.
[3] C. L. Chochos, S. A. Choulis, *Prog. Polym. Sci.* **2011**, *36*, 1326.
[4] H.-Y. Chen, J. Hou, S. Zhang, Y. Liang, G. Yang, Y. Yang, L. Yu, Y. Wu, G. Li, *Nat. Photonics* **2009**, *3*, 649.
[5] Y. Liang, Z. Xu, J. Xia, S.-T. Tsai, Y. Wu, G. Li, C. Ray, L. Yu, *Adv. Mater.* **2010**, *22*, E135.
[6] S. C. Price, A. C. Stuart, L. Yang, H. Zhou, W. You, *J. Am. Chem. Soc.* **2011**, *133*, 4625.
[7] T.-Y. Chu, J. Lu, S. Beaupré, Y. Zhang, J.-R. Pouliot, S. Wakim, J. Zhou, M. Leclerc, Z. Li, J. Ding, Y. Tao, *J. Am. Chem. Soc.* **2011**, *133*, 4250.
[8] L. Huo, S. Zhang, X. Guo, F. Xu, Y. Li, J. Hou, *Angew. Chem. Int. Ed.* **2011**, *50*, 9697.
[9] Y. Huang, X. Guo, F. Liu, L. Huo, Y. Chen, T. P. Russell, C. C. Han, Y. Li, J. Hou, *Adv. Mater.* **2012**, *24*, 3383.
[10] H. Zhou, L. Yang, A. C. Stuart, S. C. Price, S. Liu, W. You, *Angew. Chem. Int. Ed.* **2011**, *50*, 2995.
[11] Z. He, C. Zhong, X. Huang, W.-Y. Wong, H. Wu, L. Chen, S. Su, Y. Cao, *Adv. Mater.* **2011**, *23*, 4636.
[12] L. Dou, J. You, J. Yang, C.-C. Chen, Y. He, S. Murase, T. Moriarty, K. Emery, G. Li, Y. Yang, *Nat. Photonics* **2012**, *6*, 180.

[13] X. Li, W. C. H. Choy, L. Huo, F. Xie, W. E. I. Sha, B. Ding, X. Guo, Y. Li, J. Hou, J. You, Y. Yang, *Adv. Mater.* **2012**, *24*, 3046.
[14] C. E. Small, S. Chen, J. Subbiah, C. M. Amb, S.-W. Tsang, T.-H. Lai, J. R. Reynolds, F. So, *Nat. Photonics* **2012**, *6*, 115.
[15] X. Guo, C. Cui, M. Zhang, L. Huo, Y. Huang, J. Hou, Y. Li, *Energy Environ. Sci.* **2012**, *5*, 7943.
[16] J. You, X. Li, F.-X. Xie, W. E. I. Sha, J. H. W. Kwong, G. Li, W. C. H. Choy, Y. Yang, *Adv. Energy Mater.* **2012**, *2*, 1203.
[17] S. Qu, H. Tian, *Chem. Commun.* **2012**, *48*, 3039.
[18] H. Bronstein, Z. Chen, R. S. Ashraf, W. Zhang, J. Du, J. R. Durrant, P. S. Tuladhar, K. Song, S. E. Watkins, Y. Geerts, M. M. Wienk, R. A. J. Janssen, T. Anthopoulos, H. Sirringhaus, M. Heeney, I. McCulloch, *J. Am. Chem. Soc.* **2011**, *133*, 3272.
[19] J. C. Bijleveld, V. S. Gevaerts, D. Di Nuzzo, M. Turbiez, S. G. J. Mathijssen, D. M. de Leeuw, M. M. Wienk, R. A. J. Janssen, *Adv. Mater.* **2010**, *22*, E242.
[20] W. Li, W. S. C. Roelofs, M. M. Wienk, R. A. J. Janssen, *J. Am. Chem. Soc.* **2012**, *134*, 13787.
[21] L. Dou, J. Gao, E. Richard, J. You, C.-C. Chen, K. C. Cha, Y. He, G. Li, Y. Yang, *J. Am. Chem. Soc.* **2012**, *134*, 10071.
[22] Y. Li, S. P. Singh, P. Sonar, *Adv. Mater.* **2010**, *22*, 4862.
[23] M. T. Lloyd, D. C. Olson, P. Lu, E. Fang, D. L. Moore, M. S. White, M. O. Reese, D. S. Ginley, J. W. P. Hsu, *J. Mater. Chem.* **2009**, *19*, 7638.
[24] J. Zou, H.-L. Yip, Y. Zhang, Y. Gao, S.-C. Chien, K. O'Malley, C.-C. Chueh, H. Chen, A. K. Y. Jen, *Adv. Funct. Mater.* **2012**, 2804.
[25] N. Zhou, X. Guo, R. P. Ortiz, S. Li, S. Zhang, R. P. H. Chang, A. Facchetti, T. J. Marks, *Adv. Mater.* **2012**, *24*, 2242.
[26] K.-S. Chen, Y. Zhang, H.-L. Yip, Y. Sun, J. A. Davies, C. Ting, C.-P. Chen, A. K. Y. Jen, *Org. Electron.* **2011**, *12*, 794.
[27] A. Hadipour, B. de Boer, P. W. M. Blom, *Adv. Funct. Mater.* **2008**, *18*, 169.
[28] A. Hadipour, B. de Boer, J. Wildeman, F. B. Kooistra, J. C. Hummelen, M. G. R. Turbiez, M. M. Wienk, R. A. J. Janssen, P. W. M. Blom, *Adv. Funct. Mater.* **2006**, *16*, 1897.
[29] S. Kouijzer, S. Esiner, C. H. Frijters, M. Turbiez, M. M. Wienk, R. A. J. Janssen, *Adv. Energy Mater.* **2012**, 945.
[30] V. S. Gevaerts, A. Furlan, M. M. Wienk, M. Turbiez, R. A. J. Janssen, *Adv. Mater.* **2012**, *24*, 2130.
[31] I. McCulloch, R. S. Ashraf, L. Biniek, H. Bronstein, C. Combe, J. E. Donaghey, D. I. James, C. B. Nielsen, B. C. Schroeder, W. Zhang, *Acc. Chem. Res.* **2012**. *45*, 714.
[32] H. Zhou, L. Yang, S. C. Price, K. J. Knight, W. You, *Angew. Chem. Int. Ed.* **2010**, *49*, 7992.
[33] M. Heeney, W. Zhang, D. J. Crouch, M. L. Chabinyc, S. Gordeyev, R. Hamilton, S. J. Higgins, I. McCulloch, P. J. Skabara, D. Sparrowe, S. Tierney, *Chem Commun.* **2007**, 5061.
[34] S. S. Zade, N. Zamoshchik, M. Bendikov, *Chem. Eur. J.* **2009**, *15*, 8613.
[35] A. Hadipour, D. Cheyns, P. Heremans, B. P. Rand, *Adv. Energy Mater.* **2011**, *1*, 930.
[36] J. R. Matthews, W. Niu, A. Tandia, A. L. Wallace, J. Hu, W.-Y. Lee, G. Giri, S. C. B. Mannsfeld, Y. Xie, S. Cai, H. H. Fong, Z. Bao, M. He, *Chem. Mater.* **2013**, *25*, 782.
[37] C. Kanimozhi, N. Yaacobi-Gross, K. W. Chou, A. Amassian, T. D. Anthopoulos, S. Patil, *J. Am. Chem. Soc.* **2012**, *134*, 16532.
[38] F. Liu, Y. Gu, C. Wang, W. Zhao, D. Chen, A. L. Briseno, T. P. Russell, *Adv. Mater.* **2012**, *24*, 3947.
[39] J. W. Jung, F. Liu, T. P. Russell, W. H. Jo, *Energy Environ. Sci.* **2012**, *5*, 6857.
[40] T. Erb, U. Zhokhavets, G. Gobsch, S. Raleva, B. Stuhn, P. Schilinsky, C. Waldauf, C. J. Brabec, *Adv. Funct. Mater.* **2005**, *15*, 1193.
[41] H. Ohkita, S. Cook, Y. Astuti, W. Duffy, S. Tierney, W. Zhang, M. Heeney, I. McCulloch, J. Nelson, D. D. C. Bradley, J. R. Durrant, *J. Am. Chem. Soc.* **2008**, *130*, 3030.
[42] T. M. Clarke, A. M. Ballantyne, S. Tierney, M. Heeney, W. Duffy, I. McCulloch, J. Nelson, J. R. Durrant, *J. Phys. Chem. C* **2010**, *114*, 8068.
[43] T. M. Clarke, A. M. Ballantyne, J. Nelson, D. D. C. Bradley, J. R. Durrant, *Adv. Funct. Mater.* **2008**, *18*, 4029.
[44] Y. He, Y. Li, *Phys. Chem. Chem. Phys.* **2011**, *13*, 1970.
[45] E. L. Ratcliff, J. Meyer, K. X. Steirer, N. R. Armstrong, D. Olson, A. Kahn, *Org. Electron.* **2012**, *13*, 744.
[46] W. C. Tsoi, S. J. Spencer, L. Yang, A. M. Ballantyne, P. G. Nicholson, A. Turnbull, A. G. Shard, C. E. Murphy, D. D. C. Bradley, J. Nelson, J.-S. Kim, *Macromolecules* **2011**, *44*, 2944.
[47] A. Rajendran, T. Tsuchiya, S. Hirata, T. D. Iordanov, *J. Phys. Chem. A* **2012**, *116*, 12153.
[48] T. Clarke, A. Ballantyne, F. Jamieson, C. Brabec, J. Nelson, J. Durrant, *Chem. Commun.* **2009**, 89.
[49] T. M. Clarke, J. R. Durrant, *Chem. Rev.* **2010**, *110*, 6736.
[50] S. D. Dimitrov, C. B. Nielsen, S. Shoaee, P. S. Tuladhar, J. Du, I. McCulloch, J. R. Durrant, *J. Phys. Chem. Lett.* **2011**, *3*, 140.
[51] C. Deibel, T. Strobel, V. Dyakonov, *Adv. Mater.* **2010**, *22*, 4097.